Sedimentation-based confinement of individual Giant Unilamellar Vesicles in microchamber arrays with a dynamically exchangeable outer medium

Syed Kaabir Ali, Catherine Sella, Vadim Dilhas, Barbara Jacková, Marina Mariconti, Clara Gomez-Cruz, Laurent Thouin, Mathieu Morel, Damien Baigl, Ayako Yamada

Sedimentation-based confinement of individual Giant Unilamellar Vesicles in microchamber arrays with a dynamically exchangeable outer medium

Syed Kaabir Ali[1], Catherine Sella[1], Vadim Dilhas[1], Barbara Jacková[1], Marina Mariconti[1], Clara Gomez-Cruz[1], Laurent Thouin[1], Mathieu Morel[1], Damien Baigl[1], and Ayako Yamada[1]*

[1] PASTEUR, Department of Chemistry, École Normale Supérieure, PSL University, Sorbonne Université, CNRS, 75005 Paris, France

* Correspondence to: ayako.yamada@ens.psl.eu

Abstract

Giant unilamellar vesicles (GUVs) are an ideal model to study cellular membrane functions *in vitro*, yet difficult to manipulate due to their fragile nature, especially when subjected to dynamic change of their external microenvironment. Here, we introduce an original microfluidic concept for constrain-free confinement of individual GUVs in microchambers with a dynamically exchangeable outer medium. With this method, GUVs self-confine in an array of laterally separated microchambers by sedimentation, avoiding any mechanical constrain and membrane deformation while allowing time-resolved microscopy observation. A microfluidic channel above the chambers allows a diffusion-based exchange of the GUV outer medium that can be completed in a few seconds for fast-diffusing molecules to about one minute for large proteins in a viscous medium. We numerically establish the geometric and flow parameters optimizing medium exchange while preventing GUV from lifting out. We experimentally demonstrate that different aqueous solutions separated by air plugs can be flowed into the channel by taking advantage of a polydimethylsiloxane-based hydrophilic channel wall. We also exploit the possibility to manipulate microliter sample volumes and dynamically control the external environment of GUV for *in situ* observation of membrane binding protein cell-free expression. We find in particular that the membrane-targeting sequence of *Bacillus subtilis* MinD binds to GUVs and induces extensive membrane tubulation. This technically simple method offers a robust way to confine GUVs and dynamically control their outer medium, thus constituting an ideal platform to study the spatio-temporal response of reconstituted membranes and/or synthetic cell studies subjected to dynamic micro-environments.

Introduction

GUV, a cell-sized closed phospholipid bilayer membrane, has been extensively exploited as both synthetic cells and *in vitro* model of cell and cell organelle membranes.[1-4] GUVs are manipulable individually by micropipette under a precise control of membrane tension, which enables, for example, characterizing physicochemical properties of the membrane via submicron-diameter membrane tubes pulled out from a GUV for several tens of microns.[5-7] Their deformability, in turn, makes them difficult to handle in a high through-put manner, in particular, with changes of their environment. In this context, microfluidics technology has been employed to capture a large number of GUVs using microstructures.[8-11] However, those systems either are highly complex in fabrication and in manipulation, or do not allow GUVs to

undergo deformations while being trapped or being free from mechanical constraint. As we reported previously, microwells etched on the ceiling of a microfluidic channel allows us to trap and release GUVs by elastic energy gradient. However, the system is sensitive to the membrane tension of GUVs and thus not suitable for assays accompanied by GUV deflation.[9] Herein, we introduce a microfluidic concept, in which a large number of individual GUVs self-confine by sedimentation in microwells covered with channels allowing exchanges of their outer medium. The thin bottom layer of the microwells allows dynamic microscopy observations of GUVs at a high magnification, while a water reservoir placed closely above the channels prevents evaporation through the channel wall during hours of biochemical reactions, such as gene expression at 37 °C.[12]

Microwells have been widely used, for instance, to capture single or multiple cells, GUVs as mentioned above, or to reconstitute cellular architecture *in vitro*.[9, 13-16] Various materials, such as polydimethylsiloxane (PDMS), hydrogels, or UV-curable resins have been used for microwells. In this study, we establish a novel protocol of a simpler fabrication of microwells made of a photoresist, notably without the issue of autofluorescence both under visible and UV light excitation.

To enable sequential exchanges of the outer medium of GUVs in a small volume, while keeping the device immobile on a microscopy stage, air plugs can be used to separate different solutions in single tubing connected to a pump.[17, 18] However, due to the hydrophobic nature of conventional microfluidic channel surfaces, e.g., PDMS, introduction of air in a channel is usually undesired since it leaves air bubbles pinned at the channel surface. A smart solution has been proposed by Gokaltun, *et al.*, in which the PDMS surface was turned hydrophilic simply by adding a block copolymer of dimethylsiloxane and ethylene oxide to PDMS.[19] By combining those methodologies, we demonstrate that the outer medium of GUVs can be exchanged multiple times in our device under microscopy observation. Moreover, a volume of the outer medium as small as 10 µL being required, the device is advantageous for biochemical assays targeting model membranes with precious reagents. During the medium exchange, however, GUVs tend to escape from shallow microwells due to a lift force induced by the medium flow above the microwells. To find an optimal range of well depth and flow velocity, numerical simulations have been performed following the strategy used in the study on spheroid trapping by Rousset, *et al.*[20]

Lastly, the applicability of our device to *in situ* biochemical reaction in the presence of GUVs is investigated. As a proof of concept, a cell-free gene expression has been performed, which is challenging because of the high osmolality of the medium and hours of incubation process at

37 °C. A membrane-targeting sequence of Bacillus subtilis MinD, bsMTS, is expressed using the cell-free system in the presence of GUVs and is allowed to interact with their membrane. We demonstrate that YFP-conjugated bsMTS is successfully expressed in the device in the presence of GUVs and binds to the bilayer membrane containing a negatively charged lipid. Moreover, spontaneous membrane tubulation from the GUVs occurs upon the expression of YFP-bsMTS.

Results and discussion

Microfluidic device characterization

As illustrated in Figure 1a, a thin photoresist layer containing microwells was covered by a PDMS layer containing a microfluidic circuit consisting here in two parallel straight channels. To avoid evaporation through PDMS, a water reservoir was added at the vicinity of the channels, covering most of the channel areas except their extremities.[12] A photograph of the assembled microfluidic device is shown in Figure 1b. The microwells had a diameter of 40 μm and were distributed at 40 μm intervals, covering an area of 15 mm × 25 mm as illustrated in Figure S1a in Supporting Information. The two channels were designed to have a width and a length of 3 mm and 2 cm, respectively, smoothly connected to their inlets and outlets as depicted in Figure S1b in Supporting Information. Each channel covered *ca.* $1.1 \cdot 10^4$ microwells. The final depths of the microwells were smaller than the thickness of the original photoresist dry films used for a master mold fabrication due to compression during dry film lamination and PDMS mold replication processes: the wells fabricated with 50 μm- and 100 μm-thick films had a depth of 43.0 ± 0.2 μm and 91.5 ± 0.1 μm, respectively. The channels fabricated from 50 μm- and 100 μm-thick films had a final height of 46.3 ± 0.4 μm and 100.7 ± 3.2 μm, respectively, corresponding to volume channels of 3.1 μL and 6.8 μL, respectively. As described in Supporting Information, microwells were fabricated in OrmoStamp photoresist by soft lithography directly on a thin cover glass slide. Although a thin layer of the photoresist was remaining at the bottom of the microwells, its thickness, 6.5 ± 5.2 μm, was small enough to allow high magnification microscopy observations of GUVs inside the microwells. It is worth noting that the microwell layer can be fabricated rapidly in less than 20 min once a PDMS mold is obtained, and that OrmoStamp was selected as the material for the microwells among other UV sensitive resins because of its low autofluorescence both under visible and UV light excitation.

GUV trapping

GUVs containing a sucrose solution were left to sediment in an outside medium with a 1:1 (v/v) mixture of the sucrose and a glucose solution at a same osmolality. Due to the density difference, GUVs sedimented at the bottom of the channel and some of them further fell into the microwells, leading to spontaneous GUV confinement in laterally isolated microchambers with an open ceiling for medium exchange. The GUVs that remained outside the wells were carried away upon fluid exchange as depicted in Figure 1c. Figure 1d shows a representative image of GUVs composed of L-α-phosphatidylcholine from chicken egg (EPC) and a fluorescent lipid, Texas Red 1,2-dihexadecanoyl-sn-glycero-3-phosphoethanolamine (Texas Red DHPE), trapped in the microwells after the channel was rinsed with a solution without GUV. It shows that, after their sedimentation in the wells, the GUVs remained confined under the medium replacement in the upper microfluidic channels.

To estimate the necessary time for GUVs to sediment in the microwells, an evaluation following an approximation made by Haberman *et al.* was employed.[20, 21] The terminal velocity U of a sphere with a radius r moving in a still medium in an infinite cylinder with a radius R can be described as

$$U = 2/9 \cdot r^2 g(\rho_o - \rho_i)(1+\sigma)/\mu K(1+2\sigma/3)$$

where g is gravitational constant, ρ_o ($1.030 \cdot 10^3$ kg m^{-3}) and ρ_i ($1.037 \cdot 10^3$ kg m^{-3}) are the densities of the outer and inner medium of the sphere, respectively, σ is the viscosity ratio of the outer to the inner medium, μ is dynamic viscosity of the outer medium, and K is a wall correction factor, which is a function of σ and $\delta = r/R$.[21] Viscosities of 1:1 (v/v) mixture of sucrose and glucose solutions with an osmolality of 300 mOsm used for most of the experiments and 1.72 Osm used for the cell-free gene expression experiments were measured as 1.18 and 5.19 mPa s, respectively. Although lipid bilayer membranes in disordered phase are fluidic with certain viscosities,[22-26] when a GUV sediments vertically, there is no membrane flow due to the axial symmetricity that prevents circulation of lipids in the membrane.[27] We thus assumed σ = 0, which gives[21]

$$U = 2/9 \cdot r^2 g(\rho_o - \rho_i)/\mu K$$

and

$$K = (1 - 0.75857\delta^5)/(1 - 2.1050\delta + 2.0865\delta^3 - 1.7068\delta^5 + 0.72603\delta^6)$$

The graph in Figure 2a shows the value of U plotted against GUV diameter, $2r$, while the microwell diameter, $2R$, is fixed to 40 μm and μ = 1.2 (magenta). For a

comparison, the result when a GUV sediments in a still infinite medium, *i.e.*, $K = 1$, is shown in green.

In Figure 2b, the time necessary for a GUV to sediment for 40 µm in a 40 µm-diameter infinitely long cylinder, $T_{40\ \mu m}$, is plotted against GUV diameter in magenta, together with the case $K = 1$ in green. For GUVs larger than 2 µm, $T_{40\ \mu m}$ is smaller than 600 s, which is indicated with a blue line in Figure 2b. After introduction in a channel, GUVs were thus allowed to sediment for 10 min in a still medium, and this process was repeated twice. The size distribution of GUVs right after the electro-formation, with an average diameter of 4.4 ± 6.1 µm ($n = 2984$), is shown in magenta in Figure 3a. Interestingly, the peak of the size distribution of GUVs after trapping is shifted toward greater values as shown in yellow in Figure 3a, with an average diameter of 8.5 ± 5.6 µm ($n = 1471$). Due to a longer time necessary for small GUVs to sediment into microwells, GUVs with a diameter of a few µm can be excluded, in agreement with the result shown in Figure 2b. The number of GUVs trapped in single microwells was also investigated. As shown in Figure 3b, a majority of the wells contained either 0 or 1 GUV ($n = 3256$), following a Poisson distribution with $\lambda = 0.54$ as a mean number of GUV per well, as indicated with black dots. Such a trapping efficiency allows us to easily get a significant number of microwells containing single GUVs with a suitable size for microscopy observation, e.g., 15-30 µm in diameter.

Molecular diffusion in the microwells upon medium exchange

To estimate the necessary time to replace the medium in the microwells, 10 µM fluorescein in phosphate buffered saline (PBS) was firstly introduced in a 46.3 µm-high channel, then PBS without fluorescein was subsequently flowed by a micro-peristaltic pump under microscopy observation. Figure 4a shows a series of fluorescence microscopy images taken at the edge (top) and center (bottom) of the channel at different time points. The flow velocity at the center of the channel induced by the peristaltic pump was measured to be 6.49 ± 1.02 mm s^{-1} by tracking fluorescently labelled GUVs flowed in the channel in a separate experiment. Note that this flow velocity corresponds to ca. 0.90 µL s^{-1}, which is also comparable to manual injection of medium to the device by micropipette. The fluorescence intensities in microwells at different positions were measured and plotted in Figure 4b for the microwells with two different depths. The distance between the microwell center and the channel edge is indicated with the color code on the right. The fluorescence decreases rapidly in particular at the channel center (black curves) as expected in a laminar flow due to a maximal linear flow velocity at the center of the channel.

The results demonstrate that a few tens of second is enough to replace small molecules such as fluorescein in the microwells. The fluctuation in the curves is due to the fluctuation of flow velocity created by the peristaltic pump. Despite this issue, the peristaltic micro-pump is advantageous compared to a syringe pump or a pressure pump, since it can be directly placed on the microscopy stage closely connected to the device, and its flow rate as well as flow direction can be easily controlled, allowing us to control fluids swiftly without looking away from the device.

Sequential medium exchange with air plugs

Next, the possibility to sequentially introduce different mediums to the device with GUVs inside the microwells was investigated. To separate different solutions, *ca.* 10 µL air plugs were inserted between 10 µL of the solutions in a tubing connected to the peristaltic pump, as depicted in Figure 5a.[17, 18] Figure 5b shows the series of microscopy images taken at different steps, where different solutions were sequentially introduced into a 46.3 µm-high channel as follows. After GUV trapping, PBS (solution 1) was introduced in the channel as shown in the top left panel, where the fluorescence of GUVs composed of EPC and Texas Red DHPE is colored in red. Under microscopy observation, the solution was pushed throughout the channel by micropump, and replaced with air, leaving the solution 1 inside the microwells as shown in the upper, second left panel in Figure 5b. Subsequently, 10 µM fluorescein in PBS (solution 2), PBS (solution 3), and 10 µM fluorescein in PBS (solution 4) were introduced with air plugs in between. The fluorescence of fluorescein is shown in blue in Figure 5b. When the 43.0 µm-deep wells were used, a part of GUVs, in particular with a greater size, were lost during this process as shown in Figure S3 in Supporting Information. This issue was overcome by increasing the well depth. As shown in Figure 5b, with 91.5 µm-deep microwells, the majority of GUVs remained trapped after the sequential medium exchanges as indicated with white arrowheads. Importantly, when pure PDMS was initially used for the device, some microwells were covered by air that remained in the channel due to the hydrophobic nature of PDMS and OrmoStamp. To avoid the air pinning, 0.25% (w/w) dimethylsiloxane-(60-70% ethylene oxide) block copolymer (PDMS-EtO) was added to PDMS to turn the channel surface hydrophilic.[19] Therefore, with PDMS-EtO, the air plugs were smoothly moved throughout a 46.3 µm-high channel, without leaving air inside the channel as demonstrated in Figure 5c. This property was also significantly advantageous when the device was used manually without air plugs. The PDMS-EtO modification served as an effective preventive measure against the introduction of air

bubbles. Furthermore, undesired air bubble accidentally introduced in the device could be easily removed by flowing a solution with micropipette, in direct contrast to traditional PDMS featuring hydrophobic channel walls, where trapped air bubbles could potentially inflict damage on the sample and/or alter the fluid flow.

Numerical simulations of molecular diffusion and the lift force on GUVs in the microwells

Next, we evaluated molecular diffusion upon medium exchange as well as the lift force that made GUVs escape from the microwells *in silico* using COMSOL Multiphysics 6.0 software. As depicted in Figure S4 in Supporting Information, the 3D geometry of the model included 9 microwells with a depth *h* and a diameter of 40 μm were positioned at a 40 μm interval at the bottom of a 300 μm-wide, 46.3 μm-high, and 400 μm-long channel geometry. A solid sphere as a model of a GUV with a diameter *d* was positioned in the central microwell, at 1 μm distance from the microwell wall of the upstream side and of the bottom. The left panel in Figure 6a shows the evolution of average fluorescein concentration in a microwell with time, as a result of its diffusion from the well under a constant flow of medium without fluorescein introduced at the channel inlet at a velocity of 6.0 mm s-1. The well depth was varied as indicated with a color code, while the viscosity μ of the medium was set to be 1.0 mPa s. The curves for a well depth of 43.0 μm (black) and 91.5 (red) correspond to the experimental conditions shown in the left and right panel of Figure 2b with black lines, respectively. Those curves and the experimental data are plotted on a same graph in Figure S5 for direct comparison. The experimental and simulation results give similar profiles and characteristic exchange times, validating the model used for the simulations and confirming that fast-diffusing entities can be quickly exchanged in a few tens of seconds in the system. Another set of parameters was tested to simulate for a larger molecule in a viscous medium, as is the case for the cell-free gene expression experiment. For instance, the largest protein involved in the cell-free gene expression system, T7 polymerase, is 99 kDa, and the viscosity of the sugar solution to reach the same osmolarity as the cell-free system was 5.2 mPa s. As shown in the right panel in Figure 6a, a longer time is necessary for a large molecule to be carried away from the microwell with a large depth. Nonetheless, the required time falls in a range of a minute, which is negligible compared to characteristic times involved in gene expression. The micro-scale vertical confinement and the free diffusion allow a fast exchange of the outer medium of the confined GUVs, ranging from a few seconds for fast-diffusing molecules to a minute for large proteins. Next, we

established the conditions for which GUVs remained confined while subjected to a flow in the upper microfluidic channels. This was done by computing the lift force F_{lift} exerted on the GUVs by the flow and calculating the critical flow velocities, at which the lift force F_{lift} on a GUV equals the gravitational force $F_g = 4\pi r^3 g(\rho_i - \rho_o)/3$.[20] Figure 6b shows the resulting phase diagram, in which each line depicts the critical flow velocity as a function of the GUV diameter and for different well depths. Below each line, the colored regions represent the parameter ranges suitable for GUV trapping, *i.e.*, $F_{lift} \leq F_g$. In a range of typical flow velocity made by the peristaltic micro-pump or by manual pipetting, i.e., up to several mm s^{-1}, microwells with a depth of 70 μm or larger can trap GUVs at a high efficiency. This confirms the experimental results with 91.5 μm-deep wells shown in Figure 5b.

Cell-free gene expression of membrane binding protein in the presence of GUVs

Finally, the system was applied for *in situ* cell-free expression of a membrane binding protein in the presence of GUVs in the microwells. The cell-free gene expression system is composed of purified components necessary for gene transcription and expression machineries of *Escherichia coli*.[28, 29] Here, fluid manipulations were done manually by micropipette, which took *ca.* 15 - 20 s for each fluid injection. Since the cell-free gene expression system is sensitive to dilution, a combination of a larger channel height (100.7 ± 3.2 μm) and smaller well depth (43.0 ± 0.2 μm) was exploited for a better fluid exchange inside microwells, even though the GUV trapping efficiency is lower with shallow wells as shown in Figure 6a right and Figure 6b. GUVs were composed of a 4:1 (mol/mol) mixture of 1,2-dioleoyl-*sn*-glycero-3-phosphocholine (DOPC) and a negatively charged lipid, 1,2-dioleoyl-*sn*-glycero-3-phospho-(1'-rac-glycerol) (DOPG), with a small fraction of Texas Red DHPE. After GUV sedimentation, the solution in one channel was replaced with a cell-free gene expression medium containing a plasmid DNA, nucleotides, amino acids, and proteins necessary for transcription and translation machineries, as well as chaperons and disulfide bond enhancers as illustrated in Figure 7a. The same medium without plasmid DNA was introduced in the other channel. The plasmid DNA was coding for a membrane-targeting sequence (MTS) of *B. subtilis* MinD conjugated with PhiYFP (YFP-bsMTS) as its amino acid sequence depicted in Figure 7b. After introduction of the cell-free expression medium, the entire chip was incubated at 37 °C in a humidified chamber for 3.5 h prior to confocal microscopy observation. The fluorescence of the GUV membrane and YFP-bsMTS were observed with excitation wavelengths at 543

nm and 488 nm, and emission wavelengths at 599-797 nm and 518-571 nm, respectively. Surprisingly, a significant number of membrane tubes were formed from single GUVs as shown in Figure 7c, whereas in the control channel without plasmid DNA, GUVs kept their spherical shape after 3.5 h incubation at 37 °C as shown in Figure 7d. We also confirmed that in the absence of the negatively charged DOPG, YFP-bsMTS did not bind to the GUV membrane (data not shown). Spontaneous membrane tubulation from GUVs have been observed in different contexts, caused by a local charge gradient,[30-32] anchoring of amphiphilic molecules,[33] transbilayer charged lipid asymmetry,[34] or by asymmetric binding of proteins.[35, 36] MinD, together with MinC, is a key player in the positioning of division protein at midcell in *B. subtilis*.[37] It has been shown that negatively charged lipid is enriched in a spiral shape along the longitudinal axis of the bacteria and MinD colocalizes with the lipid spiral via its bsMTS that is in a shape of a-helix.[38] However, bsMTS or MinD has never been shown to create or favor a positive membrane curvature. Interestingly, Stachowiak *et al.* demonstrated that even proteins unrelated to membrane curvature can drive membrane tubulation by protein-protein crowding.[36] Our case, yet to be investigated further, may fit in this criterion.

Conclusion

We have developed a microfluidic device, with a reasonably quick fabrication protocol and of easy handling, to capture GUVs by spontaneous sedimentation into microwells at the bottom of microfluidic channels, covered with a water reservoir to avoid evaporation through the channel wall. The device allows dynamic observation of GUVs at a high magnification under sequential medium changes. The device is compatible with fluorescence microscopy observation with an excitation at UV or visible wavelength. Optimal conditions of well depths and flow velocity were searched *in silico*, supporting our experimental results. *In situ* cell-free gene expression of a membrane binding protein in the presence of GUVs was successfully performed in the device, which led to membrane tubulation from the GUVs. With optimal conditions, the device is applicable to a wide range of biochemical and biophysical assays using GUVs as a model membrane, as well as targeting other microscale objects such as colloid particles, single cells, and purified cell organelles.

Acknowledgements

This work was supported by the French National Research Agency ANR through contracts Single Nuclei on Chip via Institut Pierre-Gilles de Gennes (IPGG) (laboratoire d'excellence, Investissements d'avenir program ANR-10-IDEX-0001-02 PSL, ANR-10-LABX-31), SCDiag (ANR-21-CE18-0051). This work has benefited from the technical contribution of the joint service unit CNRS UAR 3750 (IPGG). The authors thank Drs. Nathalie Delgehyr (Institut de Biologie de l'École Normale Supérieure), Julie Plastino, Christine Gourier (Laboratoire de Physique de l'Ecole normale supérieure), and Saikat Saha (Department of Chemistry, Ecole Normale Supérieure) for fruitful discussions.

References

1. A. Roux, G. Cappello, J. Cartaud, J. Prost, B. Goud and P. Bassereau, *Proc Natl Acad Sci USA*, 2002, **99**, 5394.

2. W. Romer, L. Berland, V. Chambon, K. Gaus, B. Windschiegl, D. Tenza, M. R. E. Aly, V. Fraisier, J. C. Florent, D. Perrais, C. Lamaze, G. Raposo, C. Steinem, P. Sens, P. Bassereau and L. Johannes, *Nature*, 2007, **450**, 670-U673.

3. A. Yamada, A. Mamane, J. Lee-Tin-Wah, A. Di Cicco, C. Prevost, D. Levy, J. F. Joanny, E. Coudrier and P. Bassereau, *Nat Commun*, 2014, **5**, 3624.

4. C. Simon, R. Kusters, V. Caorsi, A. Allard, M. Abou-Ghali, J. Manzi, A. Di Cicco, D. Levy, M. Lenz, J. F. Joanny, C. Campillo, J. Plastino, P. Sens and C. Sykes, *Nat Phys*, 2019, **15**, 602.

5. D. Cuvelier, I. Derenyi, P. Bassereau and P. Nassoy, *Biophys J*, 2005, **88**, 2714.

6. S. Morlot, V. Galli, M. Klein, N. Chiaruttini, J. Manzi, F. Humbert, L. Dinis, M. Lenz, G. Cappello and A. Roux, *Cell*, 2012, **151**, 619.

7. S. Aimon, A. Callan-Jones, A. Berthaud, M. Pinot, G. E. S. Toombes and P. Bassereau, *Dev Cell*, 2014, **28**, 212.

8. T. Robinson, P. Kuhn, K. Eyer and P. S. Dittrich, *Biomicrofluidics*, 2013, **7**, 44105.

9. A. Yamada, S. Lee, P. Bassereau and C. N. Baroud, *Soft Matter*, 2014, **10**, 5878.

10. Y. Kazayama, T. Teshima, T. Osaki, S. Takeuchi and T. Toyota, *Anal Chem*, 2016, **88**, 1111.

11. N. Yandrapalli and T. Robinson, *Lab Chip*, 2019, **19**, 626.

12. A. Yamada, F. Barbaud, L. Cinque, L. Wang, Q. A. Zeng, Y. Chen and D. Baigl, *Small*, 2010, **6**, 2169.

13. J. R. Rettig and A. Folch, *Anal Chem*, 2005, **77**, 5628.

14. J. Park, B. K. Lee, G. S. Jeong, J. K. Hyun, C. J. Lee and S. H. Lee, *Lab Chip*, 2015, **15**, 141.

15. C. Stoecklin, Z. Yue, W. W. Chen, R. de Mets, E. Fong, V. Studer and V. Viasnoff, *Adv Biosyst*, 2018, **2**, 1700237.

16. S. Yamamoto, J. Gaillard, B. Vianay, C. Guerin, M. Orhant-Prioux, L. Blanchoin and M. Thery, *Embo J*, 2022, **41**, e111631.

17. B. Zheng and R. F. Ismagilov, *Angew Chem Int Ed Engl*, 2005, **44**, 2520.

18. W. A. Bauer, M. Fischlechner, C. Abell and W. T. Huck, *Lab Chip*, 2010, **10**, 1814.

19. A. Gokaltun, Y. B. A. Kang, M. L. Yarmush, O. B. Usta and A. Asatekin, *Sci Rep*, 2019, **9**, 7377.

20. N. Rousset, F. Monet and T. Gervais, *Sci Rep*, 2017, **7**, 245.

21. W. L. Haberman and R. M. Sayre, *Motion of rigid and fluid spheres in stationary and moving liquids inside cylindrical tubes*, David Taylor Model Basin Report 1143, 1958.

22. R. E. Waugh, *Biophys J*, 1982, **38**, 29.

23. R. Dimova, C. Dietrich, A. Hadjiisky, K. Danov and B. Pouligny, *Eur Phys J B*, 1999, **12**, 589.

24. A. R. Honerkamp-Smith, F. G. Woodhouse, V. Kantsler and R. E. Goldstein, *Phys Rev Lett*, 2013, **111**, 038103.

25. Y. Sakuma, T. Kawakatsu, T. Taniguchi and M. Imai, *Biophys J*, 2020, **118**, 1576.

26. H. A. Faizi, R. Dimova and P. M. Vlahovska, *Biophys J*, 2022, **121**, 910.

27. Z. H. Huang, M. Abkarian and A. Viallat, *New J Phys*, 2011, **13**, 035026.

28. Y. Shimizu, A. Inoue, Y. Tomari, T. Suzuki, T. Yokogawa, K. Nishikawa and T. Ueda, *Nat Biotech*, 2001, **19**, 751.

29. Y. Shimizu, T. Kanamori and T. Ueda, *Methods*, 2005, **36**, 299.

30. N. Khalifat, N. Puff, S. Bonneau, J. B. Fournier and M. I. Angelova, *Biophys J*, 2008, **95**, 4924.

31. Y. G. Liu, J. Agudo-Canalejo, A. Grafmuller, R. Dimova and R. Lipowsky, *Acs Nano*, 2016, **10**, 463.

32. Z. T. Graber, Z. Shi and T. Baumgart, *Phys Chem Chem Phys*, 2017, **19**, 15285.

33. I. Tsafrir, Y. Caspi, M. A. Guedeau-Boudeville, T. Arzi and J. Stavans, *Phys Rev Lett*, 2003, **91**, 138102.

34. J. Steinkuhler, P. De Tillieux, R. L. Knorr, R. Lipowsky and R. Dimova, *Sci Rep*, 2018, **8**, 11838.

35. R. L. Knorr, H. Nakatogawa, Y. Ohsumi, R. Lipowsky, T. Baumgart and R. Dimova, *PLoS One*, 2014, **9**, e115357.

36. J. C. Stachowiak, E. M. Schmid, C. J. Ryan, H. S. Ann, D. Y. Sasaki, M. B. Sherman, P. L. Geissler, D. A. Fletcher and C. C. Hayden, *Nat Cell Biol*, 2012, **14**, 944.

37. A. L. Marston, H. B. Thomaides, D. H. Edwards, M. E. Sharpe and J. Errington, *Gene Dev*, 1998, **12**, 3419.

38. I. Barak, K. Muchova, A. J. Wilkinson, P. J. O'Toole and N. Pavlendova, *Mol Microbiol*, 2008, **68**, 1315.

39. L. Mathivet, S. Cribier and P. F. Devaux, *Biophys J*, 1996, **70**, 1112.

40. M. I. Angelova and D. S. Dimitrov, *Faraday Discuss*, 1986, **81**, 303.

41. B. Ramm, P. Glock, J. Mucksch, P. Blumhardt, D. A. Garcia-Soriano, M. Heymann and P. Schwille, *Nat Commun*, 2018, **9**, 3942.

42. Z. Petrasek and P. Schwille, *Biophys J*, 2008, **94**, 1437.

43. L. He and B. Niemeyer, *Biotechnol Prog*, 2003, **19**, 544.

Figures

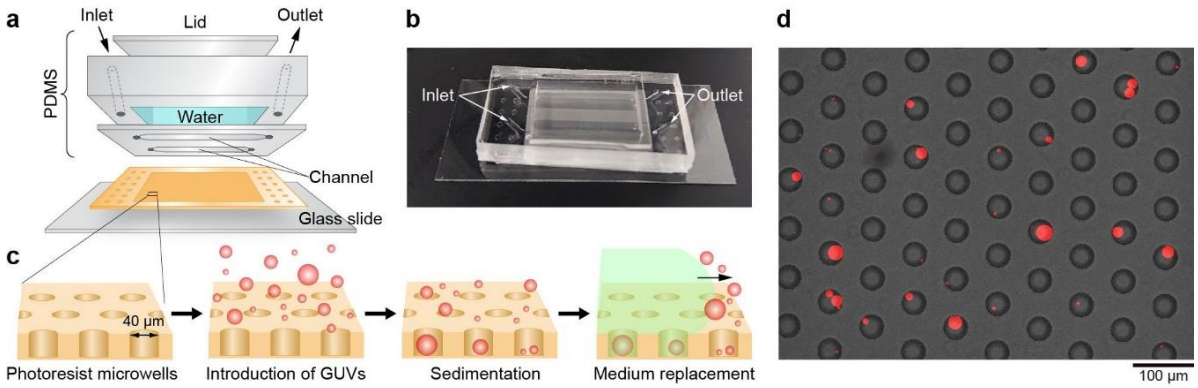

Figure 1. a) Schematic illustration of the microfluidic device composed of a microwell layer on a glass cover slide, channel and water reservoir layers made of PDMS. b) Photograph of the device. The size of the glass cover slide is 24 mm × 50 mm. c) GUVs were introduced in the channels and settled in the microwells by sedimentation. The medium outside GUVs was replaced while the GUVs were trapped in the microwells. d) Merged picture of a fluorescence microscopy image of GUVs (red) and a phase-contrast image of 43 µm-deep microwells (grey). Separate images of each channel are shown in Figure S2 in Supporting Information.

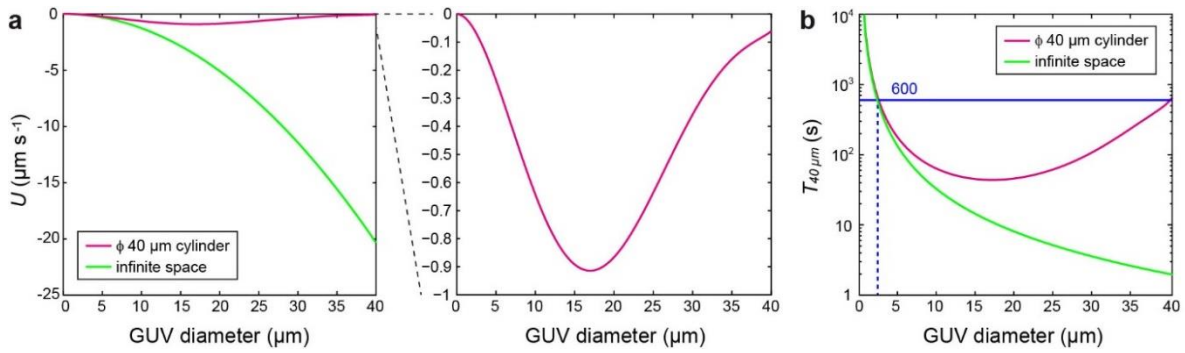

Figure 2. a) Terminal velocities *U* of a GUV sedimenting in a 40 μm-diameter cylinder (magenta) and in an infinite medium (green) are plotted against GUV diameter. The right panel shows an enlarged view of the magenta curve. b) Times necessary for a GUV to sediment for a distance of 40 μm in a 40 μm-diameter cylinder (magenta) and in an infinite medium (green) are plotted against GUV diameter. Ten minutes (blue line) is enough for a majority of GUVs to sediment for 40 μm in the cylinder.

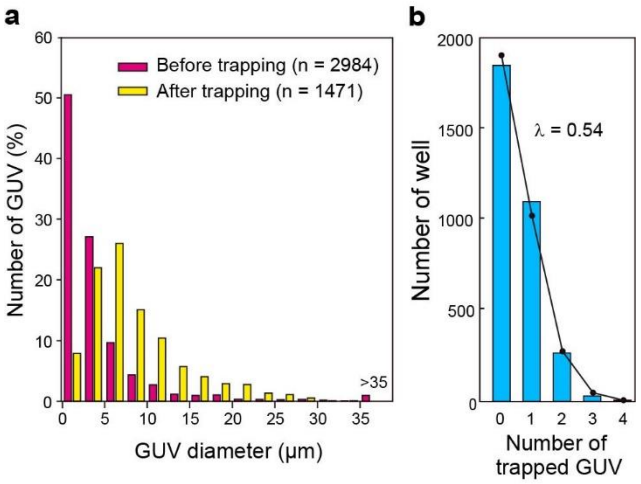

Figure 3. a) Size distribution of GUVs before (magenta) and after trapping (yellow). b) Number of microwells having trapped 0, 1, 2, 3 or 4 vesicles (n = 3256). The black dots represent expected counts of a Poisson distribution with a mean number of GUV per well, λ = 0.54.

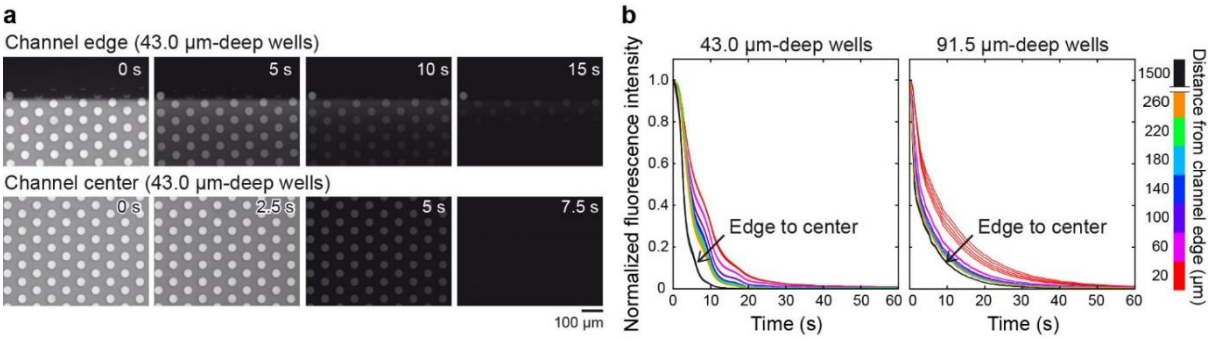

Figure 4. a) Fluorescence microscopy images of microwells at the edge of a channel (top) and at the center of the channel (bottom) at different time points under flow. The channel was initially filled with a fluorescein solution prior to the introduction at $t = 0$ of a non-fluorescent solution at a flow rate *ca.* 0.90 µL s^{-1}. b) Fluorescence intensities normalized by maximum values at $t = 0$ in the microwell areas plotted against time. The distance between the microwell center and the channel edge is indicated by the color code on the right.

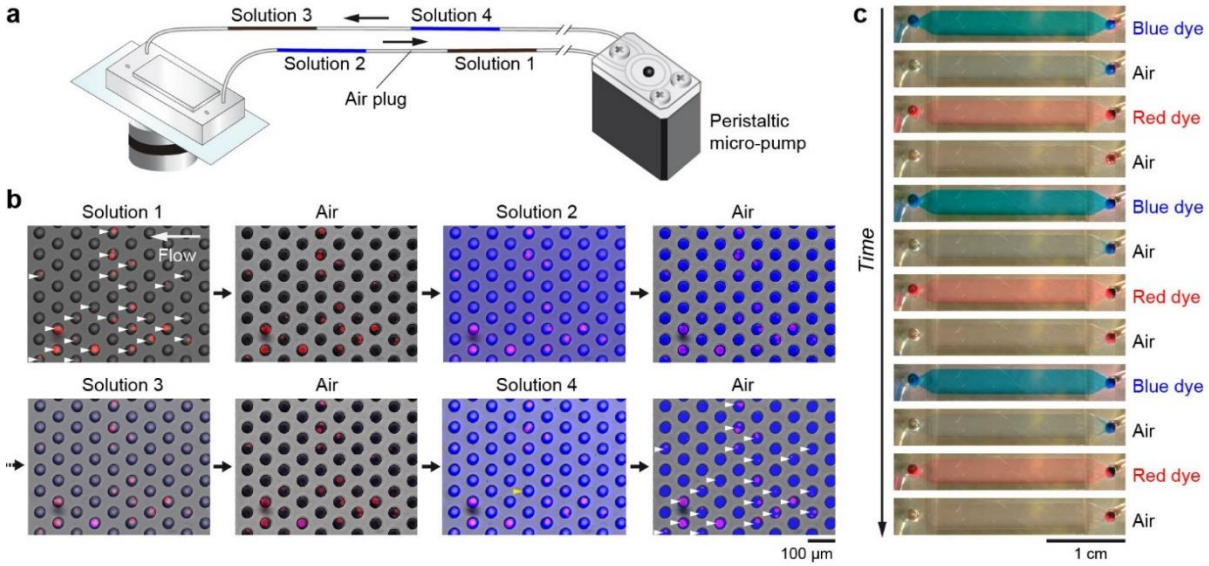

Figure 5. a) Scheme of the experimental setup. Non-fluorescent and fluorescent solutions, separated by air plugs, were introduced alternately into the microfluidic device containing GUVs by peristaltic micro-pump. b) Fluorescence microscopy images (GUV and fluorescein in red and blue, respectively) merged with phase-contrast microscopy images (grey) taken at different steps of the sequential medium exchanges using a microfluidic device with 91.5 µm-deep microwells. White arrowheads indicate the microwells containing GUVs before (top right) and after (bottom right) the medium exchanges, while a yellow arrowhead indicates a microwell where a GUV was lost during the operation. c) A series of images of an entire 46.3 µm-high channel, in which blue and red dyes separated by air plugs in a tubing were sequentially flowed by peristaltic micro-pump. Solutions were successfully exchanged without leaving air bubble in the channel.

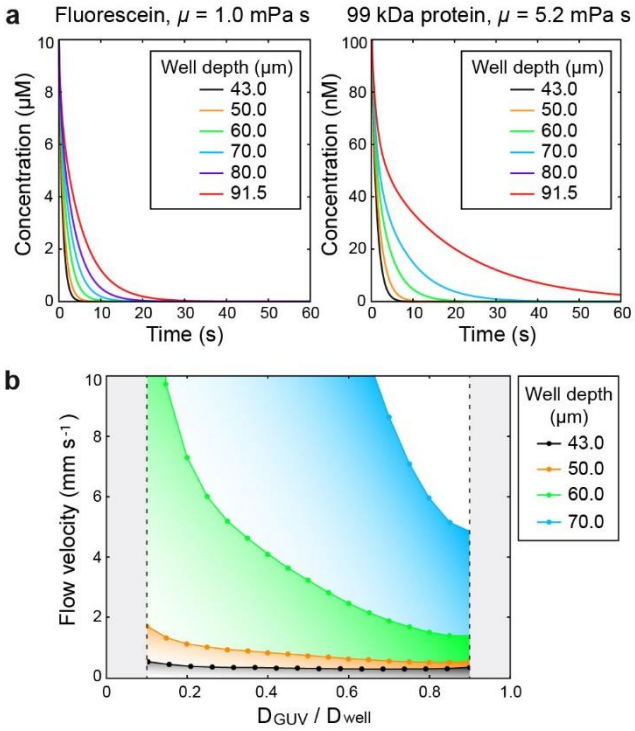

Figure 6. a) Molecular concentration change in a microwell with different depths under flow simulated by COMSOL. Results of fluorescein (diffusion coefficient $D = 4.3 \cdot 10^{-10}$ m^2 s^{-1}) in water (left) and 99 kDa protein ($D = 6.0 \cdot 10^{-11}$ m^2 s^{-1}) in a viscous medium (right), starting from an initial concentration of 10 µM and 100 nM, respectively. At $t > 0$, the same medium without fluorescein nor protein was introduced at the channel inlet at an average flow velocity fixed at 6.0 mm s^{-1}. The viscosity µ is indicated for each system. b) Phase diagram plotting critical flow velocity at which the lift force equals the gravitational force on a GUV simulated by COMSOL against the relative GUV diameter (D_{GUV}) compared to the microwell diameter (D_{well} = 40 µm) for different well depths. The viscosity of the medium was set to 1.0 mPa s.

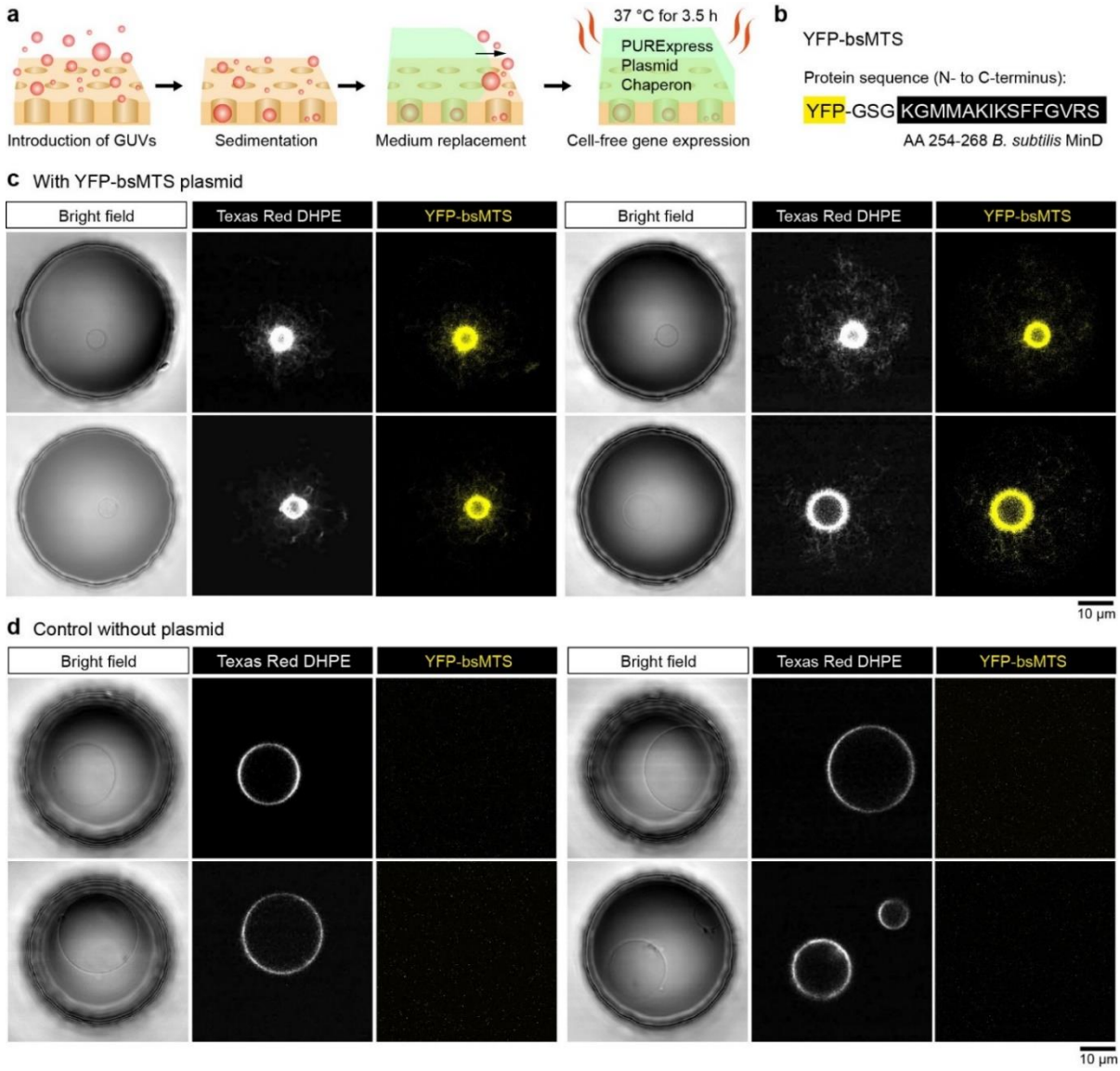

Figure 7. a) Scheme of the *in situ* cell-free gene expression in the presence of GUVs in the microfluidic device. b) Amino acid sequence of YFP-conjugated bsMTS coded on the plasmid DNA. c) Bright field images showing a microwell containing a GUV (gray), and confocal microscopy images of the GUV membrane (white), and YFP-bsMTS (yellow) after 3.5 h of gene expression at 37 °C. d) Results of the control experiment performed in the parallel channel on the same microfluidic device as c) without plasmid.